Journal of Applied Electrochemistry (2007) 37:3–14
DOI 10.1007/s10800-006-9218-8

Recovery of platinum group metals from secondary materials. I. Palladium dissolution in iodide solutions

R.J. DAWSON and G.H. KELSALL
Department of Chemical Engineering, Imperial College London, London, SW7 2AZ, UK
*(*author for correspondence, e-mail: g.kelsall@imperial.ac.uk)*

Received 23 December 2005; accepted in revised form 1 June 2006

Key words: dissolution, iodide, palladium, tri-iodide, secondary materials

Abstract

Thermodynamic predictions are reported for platinum and palladium in aqueous ammonia and iodide solutions, to define less aggressive conditions than used hitherto for leaching palladium and platinum from secondary materials. Cyclic voltammetry and amperometry of thin films of palladium, electrodeposited onto rotating vitreous carbon disc electrodes, indicated that partially oxidised adsorbed species passivated dissolution in aqueous ammonium sulfate. By contrast, dissolution rates in aqueous potassium iodide solutions were a significant fraction of that corresponding to the mass transport controlled rate of reduction of tri-iodide, which was demonstrated to be a suitable oxidant for the envisaged metal recovery process. However, iodide concentrations >1 M were required to achieve adequate solubility of the oxidation products, assumed to be PdI_4^{2-} ions, thereby avoiding inhibition by PdI_2. The reduction of tri-iodide on palladium was very facile, with large exchange current densities and Tafel coefficients; two alternative mechanisms are proposed that fitted experimental results well. In addition, a kinetic model to predict dissolution rates of Pd in tri-iodide solutions gave good agreement with experimental data, provided an equilibrium constant of $10^{-4.5}$ was used for the PdI_2/PdI_4^{2-} reaction, rather than the value of $10^{-2.8}$ derived from thermodynamic data.

Notation

d	effective thickness of PdI_2 (c) layer, m
D	diffusion coefficient, $m^2\ s^{-1}$
f	rotation rate of (ring-)disc electrode, Hz
F	Faraday constant, 96 485, C mol^{-1}
I_d	disc electrode current, A
I_r	ring electrode current, A
j	current density, A m^{-2}
j_0	exchange current density, A m^{-2}
j_L	mass transport limited current density, A m^{-2}
k_m	mass transport rate coefficient, m s^{-1}
k_i	standard rate coefficient for reaction i, m s^{-1}
K	equilibrium constant, $mol^{-1}\ dm^3$
M_{PdI2}	molar mass of PdI_2 (c), 360.23, g mol^{-1}
n	electron stoichiometric factor/reaction charge number, 1
n_d	electron stoichiometric factor/reaction charge number for disc electrode, 1
n_r	electron stoichiometric factor/reaction charge number for ring electrode, 1
N_0	collection efficiency, 1
r_1	disc electrode radius, 2.285, mm
r_2	ring electrode inner radius, 4.93, mm
r_3	ring outer radius, 5.38, mm
α	transfer coefficient, 1
β	Tafel coefficient for reduction reaction, V^{-1}
β'	Tafel coefficient for oxidation reaction, V^{-1}
δ	diffusion layer thickness, m
η	overpotential ($E - E_r$), V
ν	kinematic viscosity of 4 M KI electrolyte solution at 298 K, 0.6×10^{-6} (0.72×10^{-6} for 2 M, 0.962×10^{-6} for 0.2 M), $m^2\ s^{-1}$
θ	fractional coverage, 1
ρ_{PdI2}	density of PdI_2 (c), 6.003, g cm^{-3}
Ψ	conversion factor in equations 16, 18, 19, 21, m

1. Introduction

At US$ 12–42 per g, it is essential that platinum group metals (PGMs) are recovered from secondary sources, in which they are often in the form of thin layers, accounting for <1 wt.% of the material content. Several reviews [1, 2] have reported the different techniques for metal recovery, with most interest during the 1980s to mid 1990s, as the use of automotive exhaust catalysts increased rapidly. Three main methods have been employed: hydrometallurgical, pyrometallurgical and gas phase volatilisation. Hydrometallurgical

processes that dissolve metals selectively, leaving the support unreacted [3–5], are to be preferred, as they would minimise reagent consumption, waste production and energy consumption.

Therefore, a novel electrochemical process is being developed to dissolve PGMs selectively, using an oxidant generated at the anode of an electrochemical reactor, incorporating a cation-permeable membrane to separate anolyte and catholyte, the dissolved metal(s) being electrodeposited at the cathode. The most promising chemical systems for such a process appeared to involve ammonium salts [6] or a mixture of ammonium and iodide salts [7, 8], but hitherto they have required deployment in an autoclave at ca. 140 °C and 1 MPa oxygen partial pressure for adequate PGM dissolution rates to be achieved.

Figure 1 shows the concept of the alternative process proposed here, the only inputs being electrical energy and secondary materials, and the only outputs being de-metallised supporting material and elemental metal, with no waste streams; the chemistry merely enables the transfer of metal from support material to cathode.

2. Experimental

A rotating vitreous carbon (0.283 cm^2) disc electrode (RDE, Oxford Electrodes, Oxford, UK) and a rotating vitreous carbon (r_1 = 2.285 mm, 0.164 cm^2) disc with concentric platinum (r_2 = 4.93 mm, r_3 = 5.38 mm, 0.037 cm^2) ring (RRDE, Pine Instrument Company, Raleigh, NC, USA) were used to investigate the electrode kinetics; the latter had a collection efficiency [9] of 21.8%. Prior to experiments, the electrodes were polished with aqueous dispersions of 300 nm followed by 50 nm alumina powder, then thoroughly washed with high purity water and sonicated in an ultrasonic bath to remove any adhering particles.

All electrolytes were prepared from analytical grade chemicals and high purity water made by reverse osmosis (Elga Elgastat Prima) and de-ionisation (Elga Elgastat Maxima) to give a resistivity of 1.0×10^6 ohm m. Following reports [6, 8] of catalyst dissolution in aqueous ammonia in an autoclave, 0.25 M aqueous solutions of ammonium sulphate were made and the pH adjusted to ca. 9.5 with 25 wt.% aqueous ammonia solution. Following the solution compositions reported in the literature [7, 8, 10] for dissolution of palladium and platinum, solutions of 0.2 M KI were made initially with a natural pH of ca. 6; 2 M and 4 M KI were used in later experiments.

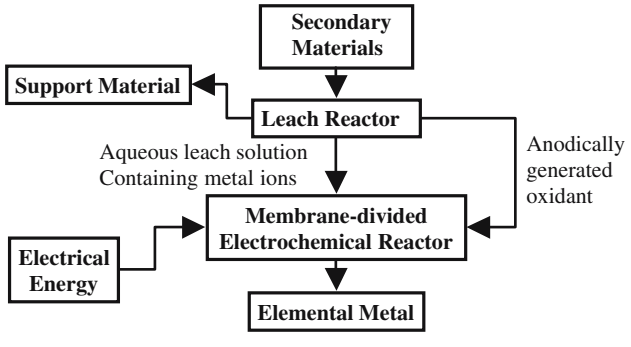

Fig. 1. Envisaged process flow diagram.

The electrochemical experiments were carried out under ambient temperatures and pressures in a three compartment glass cell, incorporating a 2 cm^2 Pt sheet counter electrode and saturated calomel reference electrode (SCE), assumed to have a potential of 0.245 V (SHE). Prior to the experiments, the electrolyte and cell were pre-purged with oxygen-free nitrogen (Domnick Hunter NG104 nitrogen generator) for at least half an hour to desorb dissolved oxygen; during experiments, nitrogen was flowed over the electrolyte surface. Electrochemical measurements were made with an Autolab Models PGstat 100 or PGstat 30 (with Bipotentiostat module) Potentiostat/Galvanostat (Eco Chemie B.V, Netherlands) controlled by a computer.

Before each experiment, the vitreous carbon disc electrodes was electrodeposited with a thin layer of palladium metal from a solution of 0.1 M tetrammine palladium chloride/1 M ammonium chloride solution at 50 °C and pH 8.5–9.5. The pH was maintained by addition of 25 wt.% aqueous ammonia solution. The most adherent, coherent and low stress deposits were achieved at 2 A m^{-2} with a nucleation stage of 200 A m^{-2} for 2 s.

The potential of the ring electrode of the RRDE was held at a value resulting in reduction of any solution species dissolved from the Pd disc electrode, enabling determination of the partial disc currents producing solution species and, by difference, those leading to surface adsorbed products.

3. Results and discussion

3.1. *Thermodynamic modelling*

Thermodynamic predictions of solubilities of various species and phases were used to screen possible leaching systems for their suitability, prior to considering the kinetics of possible chemical and electrochemical reactions in the envisaged process. The behaviours of platinum and palladium in various complexants are predicted below, as they are the most commonly used of the PGMs for a wide range of applications.

3.1.1. *Pd and Pt chloride–water systems*

Highly acidic chloride media are used in hydrometallurgical processes for the primary production and separation of PGMs; however, Figure 2 predicts stability of Pd, and to a lesser extent Pt, chloro-complexes in near neutral solutions, the equilibrium pH with their respective oxides depending on the free chloride and dissolved metal activities.

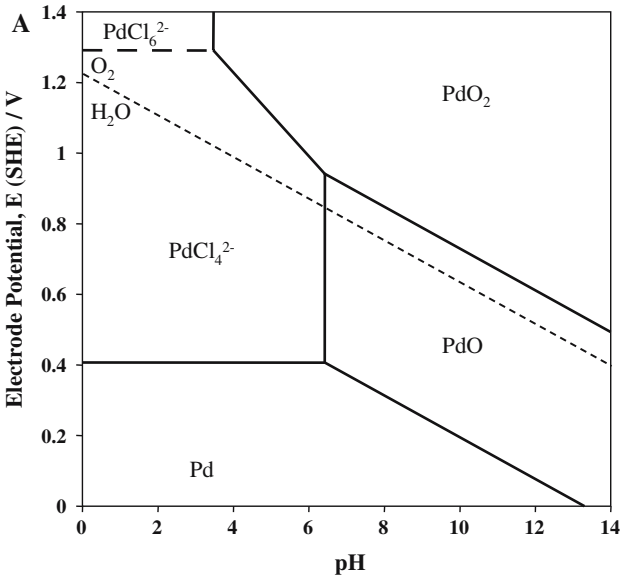

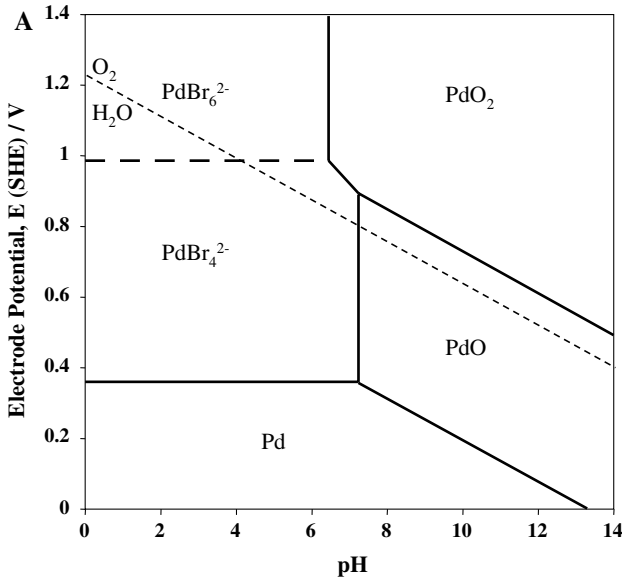

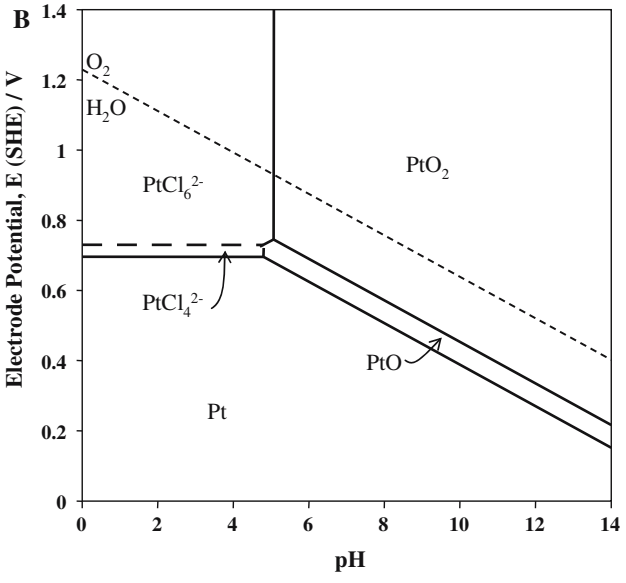

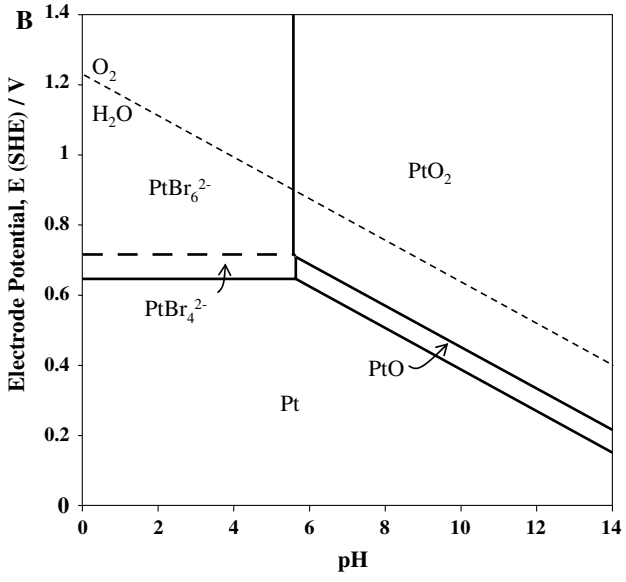

Fig. 2. Potential-pH diagrams for Pd–Cl–water and Pt–Cl–water systems at 25 °C, Cl activity 1 M, dissolved metal activities 10^{-5} M. Thermodynamic data sources: PdO, PtO, PtO_2 [11], PdO_2 calculated from [12], all other species [12].

Fig. 3. Potential-pH diagrams for Pd–Br–water and Pt–Br–water systems at 25 °C, Br activity 1 M, dissolved metal activities 10^{-5} M. Thermodynamic data sources: PdO, PtO, PtO_2 [11], PdO_2 calculated from [12], all other species [12].

3.1.2. *Pt and Pd–bromide–water systems*

As shown in Figure 3, the predicted behaviours of Pd and Pt in bromide media are similar to those in chloride media, though with slightly larger regions of stability of aqueous bromo-complex species, which extend to slightly more alkaline pHs than in chloride media.

3.1.3. *Pd and Pt–iodide–water systems*

As shown in Figure 4, the predicted behaviours of Pd and Pt in iodide are similar to those in chloride and bromide media, but the much greater stabilities of the iodo-complexes are reflected in significantly higher pHs before oxides become the more stable phases. This offers the possibility of selective dissolution of Pd and Pt over a wide pH range, especially as I_2/I_3^- species, formed by oxidation of iodide ions, could be used as oxidants.

3.1.4. *Pd and Pt–ammonia–water systems*

Figure 5, for both Pd and Pt, shows large areas of stability of ammine complexes formed in neutral and alkaline ammonia-containing media ($pK_a(NH_4^+)$ = 9.25). However, direct comparison of the diagrams for the two metals is possibly misleading, as Pd species equivalent to $Pt(NH_3)_6^{4+}$ and $Pt(NH_3)_2(OH)_2$ probably exist, but their Gibbs energies of formation do not appear to have been reported; hence, Pd^{IV} species may well be soluble in neutral and alkaline solutions. Nonetheless, the choice of oxidant would be more

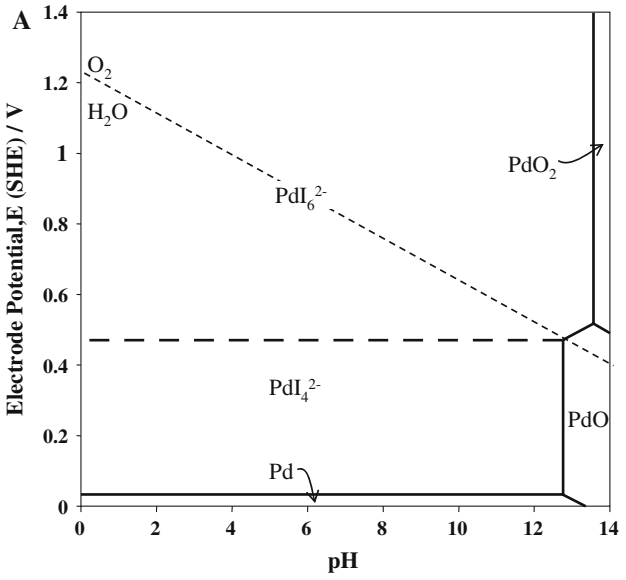

Fig. 4. Potential-pH diagrams for Pd–I–water and Pt–I–water systems at 25 °C, I activity 1 M, dissolved metal activities 10^{-5} M. Thermodynamic data sources: PdO, PtO, PtO_2 [11], PdO_2 calculated from [12], PdI_4^{2-}, PdI_6^{2-}, PtI_4^{2-}, PtI_6^{2-} [13]. All other species [12].

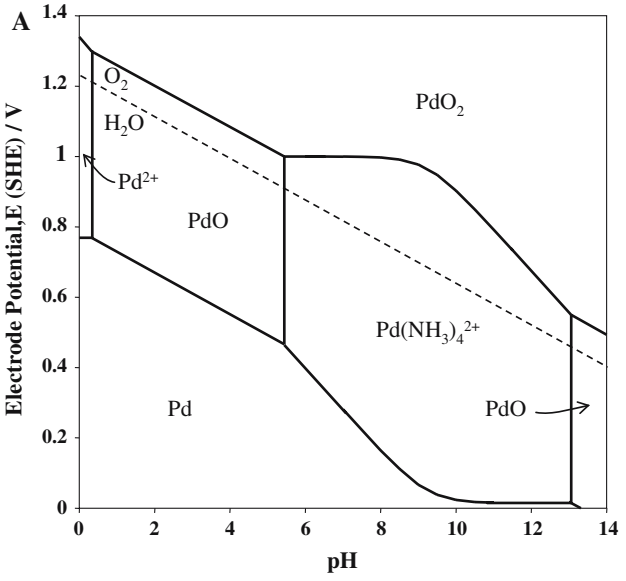

Fig. 5. Potential-pH diagrams for Pd–NH_3–water and Pt–NH_3–water systems at 25 °C, NH_3 activity 1 M, dissolved metal activities 10^{-5} M. Thermodynamic data sources: PdO, PtO, PtO_2 [11], PdO_2 calculated from [12], all other species [12].

problematic than in halide systems, especially in view of the potential oxidation of the ammonia complexant itself.

3.1.5. *Possible process chemistries*

In the process flow diagram shown in Figure 1, the reagents are recycled within the process. This requires a (strong) PGM complexant either to function as a precursor for oxidant, as for halogens formed at the anode, or to be inert to (irreversible) oxidation, unlike ammonia. In addition, the complexant must not impede electrodeposition of the metals at the cathode, the reaction regenerating complexant for recycling into the metal dissolution step. Halide systems appear particularly well suited to this specification, functioning as complexants and oxidant precursors. The standard reversible potentials of the halogens (X_3^-) decrease from chloride, to bromide to iodide, as do the metal(II) halide complex/metal reversible potentials, while oxidant solubilities in aqueous solutions increase, with consequent kinetic benefits that may compensate for the lower potential driving force, $\left(E_{X_3^-/X^-} - E_{MX_4^{2-}/M}\right)$. Figure 6 shows those differences in reversible potentials for the halide systems as functions of free halide and dissolved PGM product activities, with a constant 0.055 M trihalide oxidant activity (approximately the maximum solubility of Cl_3^-). The thermodynamics of the halide systems alone have been reported previously [14]. Though the iodide system has the lowest driving force for dissolution, this also corresponds to the lowest cell

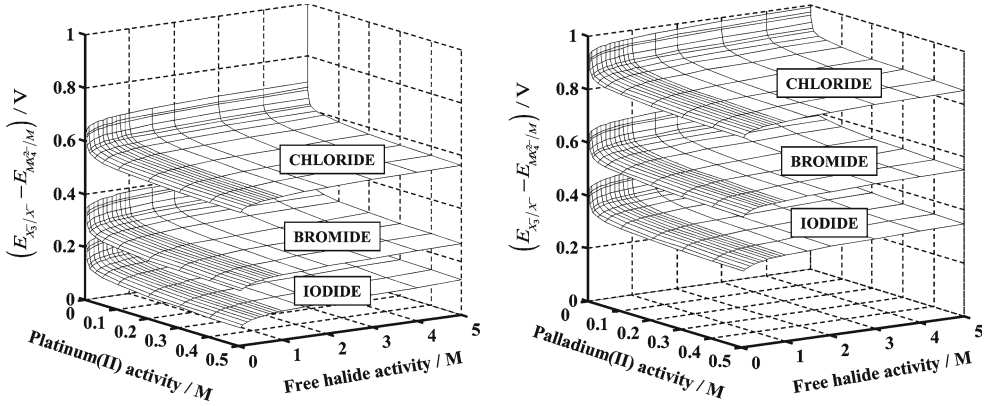

Fig. 6. Driving force (e.g., Equations (10)–(4)) for dissolution in halide media with 0.055 M tri-halide oxidant activity. Thermodynamic data sources: Halide/tri-halide [12], PGM species as stated in Figures 2–4.

voltage requirement for oxidant regeneration and metal electrodeposition.

The choice of oxidant for a process employing ammonia as complexant is less clear, but could be oxygen or a halide to provide the basis for the oxidant couple [8]. However, there are many mixed ammonia–halide Pd and Pt complexes, some of which are insoluble, and the (in)stability of ammonia to oxidation also needs to be considered. Dissolution of PGMs in less acidic and aggressive conditions could be achieved by both the iodide and ammonia systems, as the regions of Pd(II/IV) and Pt(II/IV) stabilities cover a wide pH. The iodide system appears especially apposite, having the largest areas of stability for PdI_4^{2-} and PtI_4^{2-} products, which would be formed at the lowest potentials, and the I_3^-/I^- couple is known to have fast kinetics on platinum [15]. It may be possible to leach PGMs selectively in chloride and bromide, but the pH would need to be more acidic. The potential – pH diagram for the iodide – water system is shown in Figure 7, illustrating the suitability of tri-iodide as oxidant at neutral pH.

3.2. *Palladium–ammonia electrochemistry*

3.2.1. *Cyclic voltammetry*

Figure 8 shows the current responses to sequential potential scans of a freshly prepared Pd rotating disc electrode in 0.25 M ammonium sulfate at pH 9.5.

The surface oxidation process was deactivated after only a few scans; a degree of reactivation could be achieved only by applying a strongly reducing potential for 30 s. The passivation mechanism proposed in the literature [16–18] involves sequential oxidation of adsorbed ammonia:

$$\begin{aligned} NH_{3(ads)} &\rightarrow NH_{2(ads)} + H^+ + e^- \\ NH_{2(ads)} &\rightarrow NH_{(ads)} + H^+ + e^- \\ NH_{(ads)} &\rightarrow N_{(ads)} + H^+ + e^-. \end{aligned} \quad (1)$$

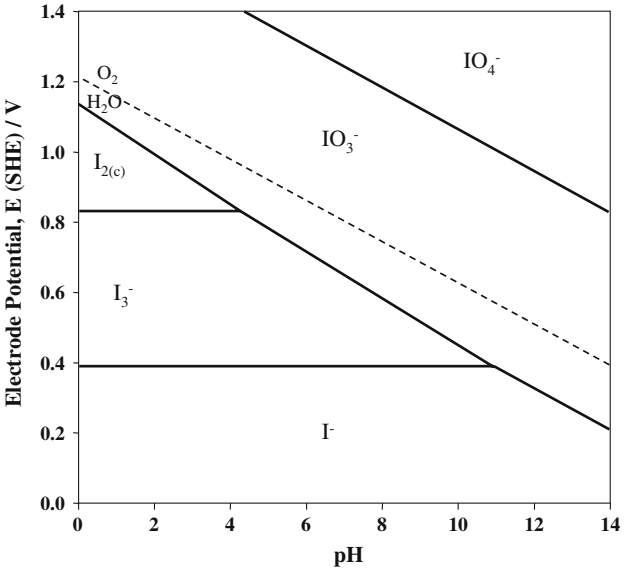

Fig. 7. Potential-pH diagram for I–water system at 25 °C, activity 1 M. Thermodynamic data sources [12].

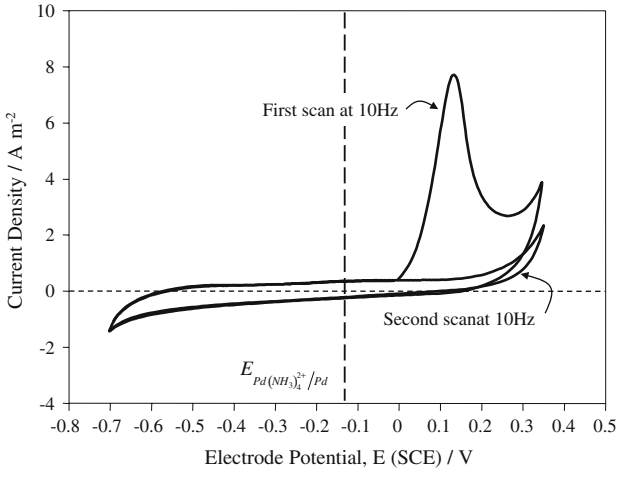

Fig. 8. Successive cyclic voltammograms of freshly electrodeposited Pd film on vitreous carbon in 0.25 M $(NH_4)_2SO_4$, scan rate 100 mV s^{-1}.

The resulting adsorbed nitrogen bonds particularly strongly in the case of 4d metals such as Pd [17] and passivates the electrode surface. This suggests that ammonia may be a less than ideal complexant for the dissolution of palladium and could partly explain why Han et al. [8] carried out the reaction in an autoclave operating at ca. 140 °C and an oxygen partial pressure of 1 MPa. Such conditions are likely to have resulted in the irreversible oxidation of ammonia, precluding its use as a regenerable complexant.

3.3. *Palladium–iodine electrochemistry*

3.3.1. *Cyclic voltammetry*

A rotating ring-disc electrode (RRDE) was used to detect palladium species, dissolved at the disc electrode, by their reduction at the Pt ring electrode. Hence, the partial disc current ($I_{d,ads}$) producing surface adsorbed species was calculated from:

$$I_{d,ads} = I_d - I_{d,diss} = I_d - \frac{I_r n_d}{n_r N_0} \tag{2}$$

where $I_{d,diss}$ and I_r are the partial disc current resulting in dissolution and the ring current, respectively (I_d being the total measured disc current), with their respective electron stoichiometric factors/reaction charge numbers, n_d and n_r.

Figure 9 shows the Pd disc and Pt ring current responses in 0.2 M KI at pH 6.5 for two consecutive potential scans at 20 mV s^{-1} with the electrode rotating at 10 Hz, the predominant oxidation reaction at potentials > − 0.3 V(SCE) being:

$$PdI_4^{2-} + 2e^- \overset{\text{ring}}{\underset{\text{disc}}{\rightleftharpoons}} Pd + 4I^- \tag{3}$$

$$E_{PdI_4^{2-}/Pd}(\text{SCE})/\text{V} = -0.063 + 0.0296\log\left(PdI_4^{2-}\right) - 0.118\log(I^-) \tag{4}$$

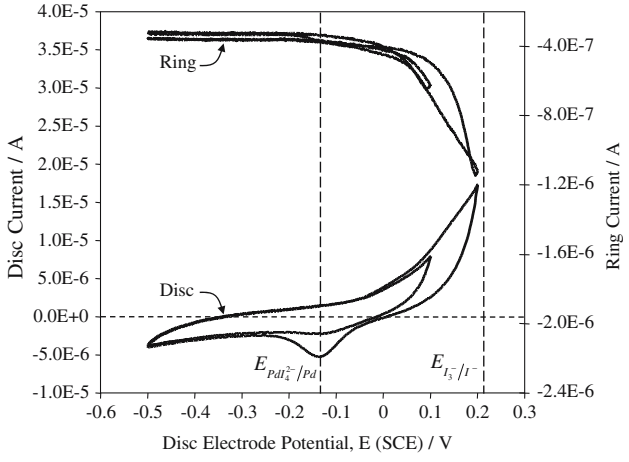

Fig. 9. Successive cyclic voltammograms of freshly plated Pd film on vitreous carbon in 0.2 M KI. Ring potential −0.3 V (SCE), pH 6.5, rotation rate 10 Hz, scan rate 20 mV s^{-1}.

However, the production of some adsorbed species on the positive-going potential sweep can be inferred by the reduction peak at − 0.1 V(SCE) on the subsequent negative-going potential sweep; the associated reduction charge grew significantly as the positive potential limit of the scan was increased, probably due to the reaction:

$$PdI_2(c) + 2e^- \rightleftharpoons Pd + 2I^- \tag{5}$$

$$E_{PdI_2/Pd}(\text{SCE})/\text{V} = -0.080 - 0.059\log(I^-) \tag{6}$$

as the solubility of PdI_2 (c) is quite low:

$$PdI_2(c) + 2I^- \rightleftharpoons PdI_4^{2-}(aq) \tag{7}$$

$$\log\left(PdI_4^{2-}\right) = -2.78 + 2\log(I^-). \tag{8}$$

Unfortunately, there appears to be a lack of agreement about Gibbs energies of formation of PdI_2 (c) and PdI_4^{2-} species in at least two sources [12, 13]; if the latter source is used, then the standard equilibrium potential in Equation (6) is − 0.0131 V (SCE) and the (molar activity-based) equilibrium constant in Equation (8) for reaction (7), is $10^{1.69}$ instead of $10^{-2.78}$. This has significant implications for the predictions of the solubility of PdI_4^{2-} ions, even though the Gibbs energies of formation data differ only by 6–18% between the sources.

The mass transport limited reduction of tri-iodide (formed adventitiously by ingress of atmospheric oxygen) contributed a steady background reduction current to the ring electrode response at − 0.3 V (SCE) by the reaction:

$$I_3^- + 2e^- \rightleftharpoons 3I^- \tag{9}$$

$$E_{I_3^-/I^-}(\text{SCE})/\text{V} = 0.2914 + 0.0296\log\left\{\left(I_3^-\right)/(I^-)^3\right\} \tag{10}$$

Taking this into account, but assuming the negative contribution to the disc current due to tri-iodide reduction was small at the potential extremes of the scan, and so shielding of the ring by the disc could be ignored, the ring current due to reduction of Pd solution species produced for both scans was only ca. 3.3–4.4% of the disc current. This equates to only ca. 15–20% of the measured disc current being used to generate dissolved PdI_4^{2-} species by reaction (3).

If the adsorbed entity was PdI_2 (c), formed by reaction (5), then using the measured charge in a potential scan to 0.2 V (SCE) and assuming a uniform layer across the surface with ρ_{PdI2} = 6.003 g cm^{-3} and M_{PdI2} = 360.23 g mol^{-1}, gives a film thickness of ca. 0.25 nm. This insoluble product, a few monolayers thick, caused rapid inhibition of the palladium dissolution during amperometric measurements.

Voltammograms of a 15.5 mm long, 0.5 mm diameter Pd wire (99.9%, Aldrich) were similar to that of the film, but the current peak for reduction of the adsorbed species was less pronounced, being masked by more apparent production of H_2/Pd_2H.

It is usual practice when dissolving PGMs in acidic chloride media to use chloride concentrations > 3 M [5, 19] to increase product solubilities and depress their equilibrium potentials, so providing a greater thermodynamic driving force for dissolution in chlorine-containing media. Therefore, the iodide concentration was increased to 2 M at a pH of ca. 6.0. Compared with Figure 9, Figure 10 shows significantly different voltammetric behaviour at the same scan rate of 20 mV s^{-1}; the current peak at ca. −0.2 V (SCE) due to reduction of adsorbed solid species, formed on the previous positive-going potential sweep, decreased greatly in the more concentrated solution. Assuming reaction (3) was operative, the collection efficiency of the ring electrode was ca. 0.196–0.201, compared with its theoretical value, (N_0 = 0.218), implying that 90–92% of the disc current was used to generate solution species, by reaction (3).

Again, assuming reaction (5) was operative, the charge associated with the reduction current peak at −0.2 V (SCE), implies the formation of PdI_2 (c) with mean thickness of ca. 0.19 nm, slightly thinner than that formed in 0.2 M KI, even though the reaction rate was much increased. Voltammograms of Pd wire were again similar to those of the thin film.

These measurements suggest that much higher steady state dissolution rates could be achieved in tri-iodide solutions with iodide concentrations ≥1 M.

3.3.2. *Amperometry*

Figure 11 shows the current–time responses to a potential step in strong iodide solutions (2–4 M) implying rapid and total dissolution of the ca. 130 nm thick Pd film. In each case, the potential applied was less negative than that of the tri-iodide couple, as calculated from Equation (10), so no iodide was oxidised in parallel with Pd dissolution. At the end of each experiment, the carbon disc electrode was clean to the naked eye, but in some cases, further inspection under a microscope showed that a few very small islands of a solid product (PdI_2) were evident in some areas around the edge of the disc, where the current density distribution would have resulted in the original Pd electrodeposit being thickest. The reduction current at the ring electrode mirrored the dissolution at the disc, indicating that the final products of the experiments were only solution species. The form of the data in Figure 11 resulted from inhibition due to PdI_2 formation causing current densities to decay with time, but at > 500 s, depending on the flux of iodide, pitting resulted in subsequent increases to maxima, reflecting maxima in surface area caused by pitting dissolution, ultimately revealing the underlying vitreous carbon. Beyond the times corresponding to the current

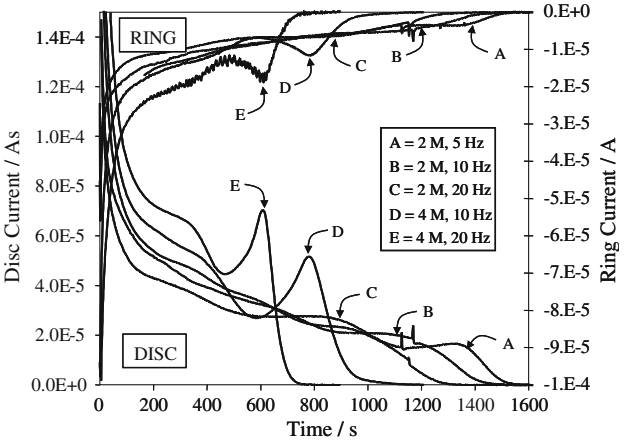

Fig. 11. Amperometric data for a freshly electrodeposited Pd film on vitreous carbon in KI with applied disc and ring potentials in 2 M KI of 0.1 V (SCE) and −0.4 V (SCE) and in 4 M KI of 0.06 V (SCE) and −0.5 V (SCE), respectively.

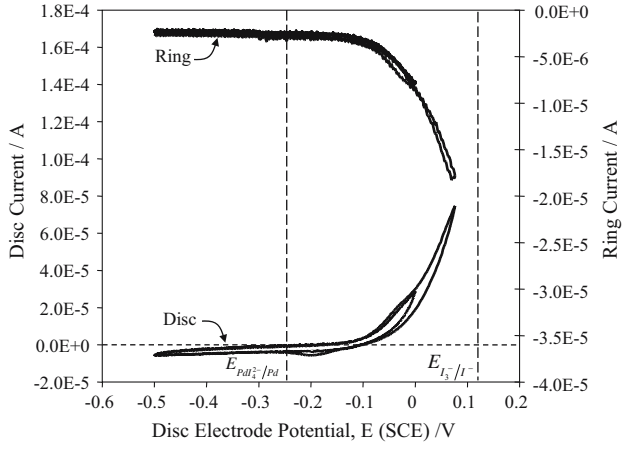

Fig. 10. Cyclic voltammogram of freshly electrodeposited Pd film on vitreous carbon in 2 M KI. Ring potential −0.4 V (SCE), pH 6.0, rotation rate 10 Hz, scan rate 20 mV s^{-1}.

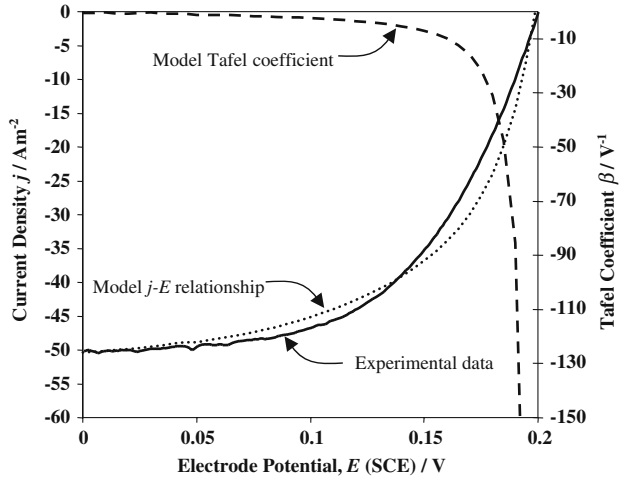

Fig. 12. Prediction of potential–current relationship from the second pathway of the kinetic model solved with Maple™, compared to experimental data for the reduction of 5.0 mM I_3^- in 2 M KI with the variation in Tafel slope overlaid.

maxima, pit growth and coalescence resulted in islands rather than holes, and hence in the area decreasing with time, until total dissolution of the Pd had occurred.

When the Pd wire electrode in 4 M KI was subjected to the same potential program, the form of the current–time data was very different to that obtained with the Pd-plated disc electrode, as the current increased slowly to a steady state, but ill defined value, due to fluctuations in mass transport rate, with obvious dark purple coloured PdI_4^{2-} product being formed. The product was identified from its absorbance maxima at 316, 408 and 485 nm; tri-iodide has absorbance maxima at 288 and 351 nm. On examination of the wire under a microscope after the experiment, the surface could be seen to be pitted and have dissolved preferentially along the scars from the wire drawing process. This would explain the observed increase in dissolution rate as the surface area increased due to pitting.

To determine the mean thickness of any PdI_2 film produced on the disc electrodes, potential pulses to −0.4 V (SCE) for 2 M and −0.5°V (SCE) for 4 M KI solutions, were applied to reduce the film at different times during experiments with the ring-disc electrode rotating at 10 Hz in 2 and 4 M KI. In both cases, the passivating PdI_2 layer was determined to be only ca. 2 nm thick at steady state, but nonetheless sufficient to affect the dissolution rate substantially. With the Pd wire electrode, unlike with the electrodeposited Pd disc electrode, the depth of material was sufficient to allow large changes in surface area due to pitting, the net effect of which was to cause an increase in current with time as dissolution occurred through a passive film.

These encouraging results indicated that the use of iodide as complexant for the dissolution of palladium is possible under mild conditions, but high iodide concentrations are required to achieve adequate solubility of the products.

3.4. *Micro-kinetic modelling of palladium dissolution in aqueous iodide solutions*

The kinetics of the oxidative dissolution of palladium in iodide by reaction (3) can be approximated by Tafel-type kinetics:

$$j_{\mathrm{Pd}} = j_{0,\mathrm{Pd}} \exp(\beta_{\mathrm{Pd}} \eta_{\mathrm{Pd}}) \tag{11}$$

From experimental data shown in Figure 10, assuming the conditions were close to steady state, values of j_0 and β were derived as 9.4×10^{-3} A m^{-2} and 27.7 V^{-1}, respectively, for a concentration of 0.01 mol m^{-3}. Similarly, for reduction of tri-iodide ions on Pd, values were determined for the exchange current density j_0 as 4.8 A m^{-2} and for the Tafel coefficient β as 67 V^{-1}, for a concentration of 5 mol m^{-3}. The value of the Tafel coefficient is experimentally difficult to establish accurately for tri-iodide reduction, due to the very fast kinetics; hence, the large values of j_0 quoted in the literature [15, 20] are subject to considerable uncertainties, as are the reported values of α. Mechanisms for the oxidation of iodide have been reported [20–23] to follow pathways via adsorbed atomic *I*, which do not appear to be plausible to explain the reduction of tri-iodide in concentrated aqueous iodide solutions. Therefore, a model for the reduction is proposed, involving unstable intermediates, either I_3^{2-} or I_2^- ions, formed by the first electron transfer step and subsequently reduced to surface adsorbed I^- ions:

Step 1:

$$\mathrm{I}^-_{3(\mathrm{bulk})} \underset{k_m}{\overset{k_m}{\rightleftharpoons}} \mathrm{I}^-_{3(\mathrm{surf})} \tag{12}$$

Step 2:

$$I^-_{3(\mathrm{surf})} + e^- \underset{k_{a1}}{\overset{k_{c1}}{\rightleftharpoons}} I^{2-}_{3(\mathrm{ads})} \quad \text{or} \quad I^-_{3(\mathrm{surf})} + e^- \underset{k_{a1}}{\overset{k_{c1}}{\rightleftharpoons}} I^-_{2(\mathrm{ads})} + I^-_{(\mathrm{surf})} \tag{13}$$

Step 3:

$$I^{2-}_{3(\mathrm{ads})} + e^- \underset{k_{a2}}{\overset{k_{c2}}{\rightleftharpoons}} 3\mathrm{I}^-_{(\mathrm{surf})} \quad \text{or} \quad I^-_{2(\mathrm{ads})} + e^- \underset{k_{a2}}{\overset{k_{c2}}{\rightleftharpoons}} 2I^-_{(\mathrm{surf})} \tag{14}$$

Step 4:

$$\mathrm{I}^-_{(\mathrm{surf})} \underset{k_m}{\overset{k_m}{\rightleftharpoons}} \mathrm{I}^-_{(\mathrm{bulk})} \tag{15}$$

A steady state mass balance on the surface species and surface coverage of adsorbed species, where θ represents the fractional coverage of intermediate $I^{2-}_{3\,(\mathrm{ads})}$ or $I^-_{2(\mathrm{ads})}$, gives:

Path 1:

$$\Psi \frac{\mathrm{d}\left[\mathrm{I}^-_{3(\mathrm{surf})}\right]}{\mathrm{d}t} = k_m\left(\left[\mathrm{I}^-_{3(\mathrm{bulk})}\right] - \left[\mathrm{I}^-_{3(\mathrm{surf})}\right]\right) - k_{c1}\left[\mathrm{I}^-_{3(\mathrm{surf})}\right](1-\theta) + k_{a1}\theta = 0 \tag{16}$$

$$\frac{\mathrm{d}\theta}{\mathrm{d}t} = k_{c1}(1-\theta)\left[I^-_{3(\mathrm{surf})}\right] - k_{a1}\theta - k_{c2}\theta + k_{a2}(1-\theta)\left[I^-_{(\mathrm{surf})}\right]^3 = 0 \tag{17}$$

$$\Psi \frac{\mathrm{d}\left[I^-_{(\mathrm{surf})}\right]}{\mathrm{d}t} = k_m\left(\left[I^-_{(\mathrm{bulk})}\right] - \left[I^-_{(\mathrm{surf})}\right]\right) + k_{c2}\theta - k_{a2}(1-\theta)\left[I^-_{(\mathrm{surf})}\right]^3 = 0 \tag{18}$$

Path 2:

$$\Psi \frac{\mathrm{d}\left[I^-_{3(\mathrm{surf})}\right]}{\mathrm{d}t} = k_m\left(\left[I^-_{3(\mathrm{bulk})}\right] - \left[I^-_{3(\mathrm{surf})}\right]\right) - k_{c1}\left[I^-_{3(\mathrm{surf})}\right](1-\theta) + k_{a1}\theta\left[I^-_{(\mathrm{surf})}\right] = 0 \tag{19}$$

$$\frac{d\theta}{dt} = k_{c1}(1-\theta)\left[I_{3(surf)}^{-}\right] - k_{a1}\theta\left[I_{(surf)}^{-}\right] - k_{c2}\theta + k_{a2}(1-\theta)\left[I_{(surf)}^{-}\right]^2 = 0 \quad (20)$$

$$\Psi\frac{d\left[I_{(surf)}^{-}\right]}{dt} = k_m\left(\left[I_{(bulk)}^{-}\right] - \left[I_{(surf)}^{-}\right]\right) + k_{c2}\theta - k_{a2}(1-\theta)\left[I_{(surf)}^{-}\right]^2 = 0 \quad (21)$$

where Ψ is a factor for converting from 3D to 2D concentration.

The rate coefficients for the electron transfer steps are defined as follows:

$$k_{c1} = k_{c1'}\exp\{-\alpha_1 FE/RT\} \quad (22)$$

$$k_{c2} = k_{c2'}\exp\{-\alpha_2 FE/RT\} \quad (23)$$

$$k_{a1} = k_{a1'}\exp\{(1-\alpha_1)FE/RT\} \quad (24)$$

$$k_{a2} = k_{a2'}\exp\{(1-\alpha_2)FE/RT\} \quad (25)$$

Therefore, current densities for the overall reaction are defined in each case as:

Path 1:

$$j = -F\left(k_{c1}(1-\theta)\left[I_{3(surf)}^{-}\right] - k_{a1}\theta + k_{c2}\theta - k_{a2}\left[I_{(surf)}^{-}\right]^3\right) \quad (26)$$

Path 2:

$$j = -F\left(k_{c1}(1-\theta)\left[I_{3(surf)}^{-}\right] - k_{a1}\theta\left[I_{(surf)}^{-}\right] + k_{c2}\theta - k_{a2}\left[I_{(surf)}^{-}\right]^2\right) \quad (27)$$

Using Maple™ mathematical software, it is possible to solve for the unknown surface concentrations and adsorbed species as functions of E, using estimates of the rate coefficients for forward and reverse reactions. Substitution of those solutions into equations (26) and (27) gives the current density–potential relationship. The solution to both pathways can be fitted to experimental data for tri-iodide reduction with very similar values of rate coefficients. For pathway 2, approximate values of $k_{c1'} = 3.2 \times 10^2$ dm s^{-1}, $k_{c2'} = 4 \times 10^5$ s^{-1}, $k_{a1'} = 5.2 \times 10^{-6}$ dm s^{-1}, and $k_{a2'} = 1.5 \times 10^{-5}$ mol^{-1} dm^4 s^{-1} were used. Figure 12 shows the result of the kinetic model via the second pathway, compared to experimental current density–potential data, and with Tafel coefficient values also plotted as a function of potential. These results are congruous with the Tafel coefficient of 67 V^{-1} estimated from experimental data.

An Evans diagram for the corrosion process was plotted using the reduction of tri-iodide via pathway 2 and the Butler-Volmer equation (28) for the metal oxidation reaction, with the exchange current densities and Tafel coefficients determined experimentally, and allowing for mass transport limitations resulting in limiting current densities for the oxidation ($j_{L,R}$) and reduction ($j_{L,O}$) processes:

$$j = \frac{j_0[\exp(\beta'\eta) - \exp(-\beta\eta)]}{\left[1 + \left(j_0/j_{L,R}\right)\exp(\beta'\eta) + \left(j_0/j_{L,O}\right)\exp(-\beta\eta)\right]} \quad (28)$$

Figure 13 shows a family of potential-current density curves for Pd in 4 M iodide + 1 mM tri-iodide, and different mass transport/rotation rates of the disc electrode, according to Levich's equation [9].

The solid line represents the kinetics of a clean Pd surface not limited by PdI_2 formation that intersects the dotted lines for tri-iodide reduction at points corresponding to the initial corrosion potentials and rates (illustrated for 10 Hz by a circle). However, the effect of restricted rates of transport of dissolved Pd^{II} species away from the Pd surface, covered by PdI_2, results in the set of dashed lines for different rotation rates. This demonstrates how corrosion potentials increase until the rate becomes kinetically controlled with respect to tri-iodide reduction. The transport limit for palladium dissolution was calculated using the equilibrium relationship between PdI_2/PdI_4^{2-} (reaction (7)) not as defined by equation (8), but using a value of −4.5 for log(K), chosen as it explains results reported below; such a value is not unreasonable considering the uncertainty of some of the thermodynamic data, as discussed above.

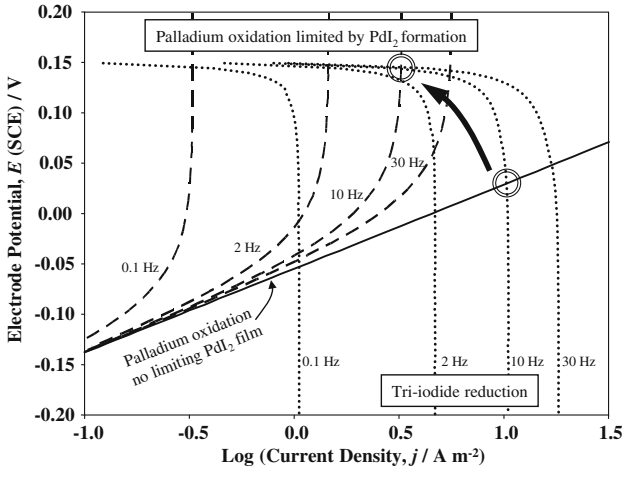

Fig. 13. Evans diagram for predicted corrosion rate and potential in 1.0 mM I_3^- and 4 M KI, mass transport rates equivalent to 10 Hz disc rotation.

3.5. *Chemical dissolution of palladium in tri-iodide/iodide*

A rotating vitreous carbon disc electrode was electrodeposited with Pd, then allowed to oxidise in a solution of 4 M iodide and 1 mM tri-iodide, whilst its electrode potential was monitored, resulting in the data shown in Figure 14. At 10 Hz, corrosion began at ca. − 0.005 V (SCE), close to the model prediction shown in Figure 13, but the potential increased rapidly, as the PdI_2 film thickened to a steady state value; these data were used to define log(K) in the model above. The overall reaction corresponds to dissolution by:

$$Pd + I_3^- + I^- \rightarrow PdI_4^{2-} \tag{29}$$

The equilibrium potential for the I_3^-/I^- couple and its fast reduction kinetics ensured that the corrosion potential was not so high as to produce Pd^{IV} species, for which:

$$PdI_6^{2-} + 2e^- \rightleftharpoons PdI_4^{2-} + 2I^- \tag{30}$$

$$E_{PdI_6^{2-}/PdI_4^{2-}}(\mathrm{SCE})/\mathrm{V} = 0.225 + 0.0296 \log\left\{\left(PdI_6^{2-}\right)/\left(PdI_4^{2-}\right)\right\} - 0.059\log(I^-) \tag{31}$$

If the electrodeposit thickness was increased, the time corresponding to the steady state Pd corrosion potential also increased. As predicted in Figure 13 and as shown in Figure 14, decreasing the mass transport rate/rotation rate from 10 Hz to 0.1 Hz, had the effect of decreasing the corrosion potential significantly, but thereafter the potential increased again, as the PdI_2 film thickened. When the mass transport/rotation rate was increased by stepping the rotation rate to 2 Hz, there was a step in potential (as predicted in Figure 13), corresponding to a greater corrosion rate. However, at this increased dissolution rate, the steady state thickness of the PdI_2 film formed was greater than at the lower rate, so that the corrosion potential increased as the layer thickened further.

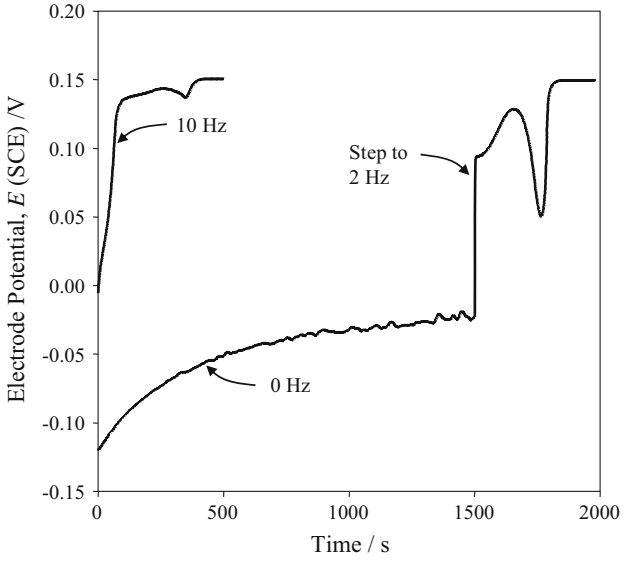

Fig. 14. Potential (SCE) of a corroding freshly electrodeposited Pd film on vitreous carbon electrodes in 1.0 mM I_3^- and 4 M KI.

The decrease in potential for ca. 100–150 s in both sets of data in Figure 14, appeared to be independent of initial electrodeposit thickness, but the extent of the decrease was affected significantly by mass transport rates. Once all the Pd metal had dissolved, the exposed vitreous carbon surface would then act as a potentiometric sensor for reaction (9), its Nernst equation being defined by equation (10). If a (porous) solid product with limited solubility, such as PdI_2, accumulated during the dissolution process, it would act as a diffusion barrier, restricting mass transport both to and from the electrode. Though the carbon electrode potential would be determined by Equation (10), it would sense not the bulk composition, but the local composition subject to restricted mass transport rates, especially of I_3^- ions. Hence, were it a Nernstian effect, then according to Equation (10), the decrease in electrode potential shown in Figure 14 for 100–150 s, would represent a change in $(I_3^-)/(I^-)$ activity ratio of ca. 1.5×10^{-4} for the 10 Hz case and 2.5×10^{-4} for the 2 Hz case. Alternatively, the decrease in potential could be interpreted in terms of the effect of decreasing I_3^- mass transport rates on the mixed potential shown in Figure 13.

If the electrodeposition produced by the same method gave repeatable film thicknesses, determined from the stripping charge, then the average corrosion current density was 6.52 A m^{-2} for the 10 Hz experiment for which results are shown in Figure 14. Figure 13 predicts an initial corrosion rate of 10.2 A m^{-2} at 10 Hz decreasing to 3.2 A m^{-2} as PdI_2 forms on the surface. This agrees well with the average value obtained experimentally, particularly considering that for the first part of the corrosion process, the rate will be almost constant at the higher value, since the reaction is initially mass transport limited with respect to tri-iodide reduction.

Using the kinetics determined for tri-iodide reduction, a plot similar in shape to that of Figure 11 can be made from the potential-time data at 10 Hz of Figure 14, but with a mass transport limited section (constant dissolution rate) for the first 57 s. Again, this is congruous with the prediction of a process switching from being mass transport to kinetically limited; however, this assumes that the rate of tri-iodide reduction is unaffected by the presence of a PdI_2 film and so can be related directly to Pd dissolution.

The molar fluxes for steady state dissolution by reaction (29) equate to zero:

$$\overrightarrow{N}_{PdI_4^{2-}} + \overrightarrow{N}_{I_3^-} + \overrightarrow{N}_{I^-} = 0 \tag{32}$$

$$-D_{PdI_4^{2-}}\frac{\partial\left[PdI_4^{2-}\right]}{\partial x} - D_{I_3^-}\frac{\partial\left[I_3^-\right]}{\partial x} - D_{I^-}\frac{\partial[I^-]}{\partial x} = 0 \tag{33}$$

Assuming reduction of I_3^- ions is transport controlled, $[I_3^-]_{x=0} = 0$, and in the absence of an adsorbed PdI_2 film:

$$\overrightarrow{N}_{I_3^-} = -\frac{D_{I_3^-}}{\delta}\left[I_3^-\right]_{x=\delta} \tag{34}$$

At steady state:

$$-D_{I^-}\left.\frac{\partial[I^-]}{\partial x}\right|_{x=\delta} = \frac{j}{F} \tag{34}$$

$$D_{I_3^-}\left.\frac{\partial\left[I_3^-\right]}{\partial x}\right|_{x=d} = -D_{PdI_4^{2-}}\left.\frac{\partial\left[PdI_4^{2-}\right]}{\partial x}\right|_{x=\delta} = \frac{j}{2F} \tag{35}$$

PdI_4^{2-} ions, rather than PdI_2 (c), will form if:

$$[I^-]_{x=0} > \left(\left[PdI_4^{2-}\right]/K\right)^{0.5} \tag{36}$$

where the equilibrium constant, $K = 10^{-2.78}$, is defined in Equation (8) or the modified value obtained from experimental data, as discussed at the end of Sec. 3.4. From Equations (35) and (11):

$$\left[PdI_4^{2-}\right]_{x=0} = \left[PdI_4^{2-}\right]_{x=\delta} + \frac{\delta j_{0,Pd}\exp(\beta_{Pd}\eta_{Pd})}{2FD_{PdI_4^{2-}}} \tag{37}$$

$$\left\{\frac{\left[PdI_4^{2-}\right]_{x=\delta} + \frac{\delta j_{0,Pd}\exp(\beta_{Pd}\eta_{Pd})}{2FD_{PdI_4^{2-}}}}{K}\right\}^{0.5} < [I^-]_{x=0} \tag{38}$$

$$[I^-]_{x=0} = [I^-]_{x=\delta} - \frac{\delta j_{0,Pd}\exp(\beta_{Pd}\eta_{Pd})}{FD_{I^-}} \tag{39}$$

$$\left\{\frac{\frac{\delta j_{0,Pd}\exp(\beta_{Pd}\eta_{Pd})}{2FD_{PdI_4^{2-}}} + \left[PdI_4^{2-}\right]_{x=0}}{K}\right\}^{0.5} + \frac{\delta j_{0,Pd}\exp(\beta_{Pd}\eta_{Pd})}{FD_{PdI_4^{2-}}} < [I^-]_{x=\delta} \tag{40}$$

where diffusion layer thicknesses (δ) may be calculated from Levich's equation [10]:

$$\delta = \left(1.554D^{-1/3}\nu^{-1/6}f^{1/2}\right)^{-1} \tag{41}$$

If thermodynamic data are used from Bard and Parsons [12] or Goldberg and Hepler [13] then, Equation (40) predicts Pd(II) solubility as PdI_4^{2-} ions, rather than PdI_2 film formation, for all iodide concentrations used in the experiments for which results are reported here. However, if K is assigned a value of $10^{-4.5}$, for reasons discussed in Sec. 3.4, then PdI_2 film formation is predicted for all conditions used, as suggested by the experimental results. This implies that there is either error in the thermodynamic data, suggested by the variations in the values reported, or that there is a strong chemical interaction leading to the formation of adsorbed iodide under nearly all conditions; potentiostatic current-time transients may help to elucidate the nature of that interaction.

4. Conclusions

(a) Platinum and palladium are predicted to form stable solution species in halide and ammoniacal solutions.
(b) The use of ammonia as complexant for the dissolution appears inappropriate, as oxidation of the ammonia passivated the palladium surface with adsorbed atomic nitrogen species.
(c) Palladium can be dissolved in iodide solutions using tri-iodide as oxidant without the need for aggressive conditions. However, the concentration of iodide required is > 1 M to achieve adequate solubility of the Pd(II) products.
(d) An inhibiting layer, probably PdI_2 (c), ca. 2 nm thick, developed during dissolution in iodide solutions, but was not greatly affected by mass transport or iodide concentrations above a threshold concentration.
(e) The reduction of tri-iodide on palladium is very facile, with large exchange current densities and Tafel coefficients. Two different mechanisms are proposed that appear to fit experimental results well, but further refinement is required before the validity of each mechanism can be established.
(f) A model to predict the dissolution rate of palladium in iodide/tri-iodide solutions gave good agreement with experimental data, provided an equilibrium constant of $10^{-4.5}$ was used for the PdI_2/PdI_4^{2-} reaction, rather than the value of $10^{-2.78}$ derived from thermodynamic data in the literature.

Acknowledgements

The authors thank the UK Engineering and Physical Sciences Research Council and the Resource Efficiency Knowledge Transfer Network for a studentship for RJD.

References

1. R.K. Mishra, *Precious Metals '89. The Metallurgical Society* (Warrendale, PA, USA, 1989) 483 pp.
2. J.E. Hoffmann, *Precious and Rare Metal Technologies*. (Elsevier, BV, 1988) 345 pp.

3. V.I. Lakshmanan and J. Ryder, (1988) *Precious and Rare Metal Technologies* (Elsevier, BV, J.) 381 pp.
4. J.A. Bonucci and P.D. Parker, *Precious Metals Mining, Extraction and Processing* (The Metallurgical Society, Warrendale, PA, USA, 1984), 27 pp.
5. T.N. Angelidis, *Top. Catal.* **16** (2001) 419.
6. X. Meng and K. Han, *Miner. Metall. Process.* **15** (1998) 36.
7. X. Meng and K. Han, *EPD Congress 1996*. (The Minerals, Metals and Materials Society, Warrendale, PA, USA, 1996) 36 pp.
8. X. Meng and K. Han, *Third International Symposium, Recycling of Metals and Engineered Materials* (The Minerals, Metals and Materials Society, Warrendale, PA, USA, 1995) 501 pp.
9. W. Albery and M. Hitchman, *Ring-Disc Electrodes* (Clarendon Press, Oxford University Press, UK, 1971) 22 pp.
10. J.C. Choi and W.H. Lee, *Han'guk Chawon Konghak Hoechi* **32** (1995) 357.
11. J. Mansikka-aho and A. Roine, *HSC Chemistry 5.11*, Outokumpu Research, http://www.outokumputechnology.com, (2003).
12. A.J. Bard, R. Parsons and J. Jordan, *Standard Potentials in Aqueous Solution* (Dekker, New York, USA, 1983) 321 pp.
13. R.N. Goldberg and L.G. Hepler, *Chem. Rev. (Washington, DC, U.S.)* **68** (1968) 229.
14. G.H. Kelsall, N.J. Welham and M.A. Diaz, *J. Electroanal. Chem.* **36** (1993) 13.
15. A.J. Bard. Iodine and Astatine, *in* A.J. Bard and M. Stratmann (Eds), Encyclopaedia of Electrochemistry B2, (Wiley, Weinheim, DE, 1985), pp. 104–145.
16. B.A.L. de Mishima, D. Lescano, T.M. Holgado and H.T. Mishima, *Electrochim. Acta* **43** (1998) 395.
17. A.C.A. de Vooys, M.T.M. Koper, R.A. van Santen and J.A.R. van Veen, *J. Electroanal. Chem.* **506** (2001) 127.
18. F.J. Vidal-Iglesias, N. Garcia-Araez, V. Montiel, J.M. Feliu and A. Aldaz, *Electrochem. Commun.* **5** (2003) 22.
19. D.R. Tyson and R.G. Bautista, *Sep. Sci. Technol.* (1987) 1149.
20. L.M. Dane, L.J.J. Janssen and J.G. Hoogland, *Electrochim. Acta* **13** (1968) 507.
21. V.A. Macagno, M.C. Giordano and A.J. Arvia, *Electrochim. Acta* **14** (1969) 335.
22. A. Hauch and A. Georg, *Electrochim. Acta* **46** (2001) 3457.
23. L. Bay, K. West, B. Winther-Jensen and T. Jacobsen, *Sol. Energy Mater. Sol. Cells* **90** (2006) 341.